Journal of Molecular Structure 1320 (2025) 139680

Contents lists available at ScienceDirect

Journal of Molecular Structure

journal homepage: www.elsevier.com/locate/molstr

Development of benzenesulfonamide containing 1,2,3-triazole and 1,3,4-oxadiazole hybrids as cathepsin B inhibitors and DFT calculations

Chander [a,1], Monika [a,1], Prabhjot Kaur [b], Laxmi [a], Neera Raghav [b,*], Pawan K. Sharma [c,d], Sita Ram [a,*]

[a] Department of Chemistry, J.C. Bose University of Science and Technology, YMCA, Faridabad 121006, India
[b] Department of Chemistry, Kurukshetra University, Kurukshetra, Haryana 136119, India
[c] Department of Chemistry, Central University of Haryana, Mahendergarh 123031, India
[d] Visiting Professor, Department of Chemistry, Wesleyan University, Middletown, CT, USA

ARTICLE INFO

Keywords:
1,2,3-Triazoles
1,3,4-Oxadiazoles
Benzenesulfonamides
Anti-cathepsin activity
Structure-activity relationship

ABSTRACT

A series of twenty-one novel hybrids of 1,2,3-triazole, 1,3,4-oxadiazole, and benzenesulfonamide motifs has been synthesized and evaluated for inhibitory potency against cathepsin B (EC 3.4.22), a cysteine protease lysosomal enzyme. The most potent anti-cathepsin B compounds **9d-f** were docked with the cathepsin B enzyme and free energy of binding as well as interactions involved in protein-ligand complex are reported. ADMET parameters of **9d-f** were calculated to check the drug-likeness behavior as orally administrative drug candidates. HOMO-LUMO energies as well as values of other global reactivity parameters were also calculated for all the twenty-one target molecules using DFT calculations. The investigated compounds have possessed excellent inhibition potential against cathepsin B enzyme with 40.50 -76.64 % inhibition at 10^{-8} M concentrations as compared to curcumin (% inhibition = 32.46 % at 10^{-8} M concentration), the reference taken. Further, the docking obtained results were found in agreement with the experimentally observed higher anti-cathepsin activity of **9e** among the docked compounds. ADMET calculations proved the compounds **9d-f** as safer orally administrative drug candidates. DFT results suggest that the compounds of series **9** are better electron acceptors than their respective analogues in series **10** which in turn are better electron acceptors than their respective analogues in series **11**.

1. Introduction

Belonging to the family of papain enzymes, cathepsins are a group of lysosomal proteases having their presence in mammalian cells and are responsible for various pathological functions within the cells such as immune response, protein degradation, energy metabolism, etc. [1-3]. Contemporarily to the presence of cathepsins within the cells, recent research work has shown them to be present outside the cells also and are responsible for various extracellular functions [4]. Overexpression of extracellular cathepsins, especially cathepsin B (EC 3.4.22), a cysteine protease lysosomal enzyme, plays a crucial role in various types of pathological as well as oncogenic processes in living beings [5,6]. The carboxyl peptidase activity of cathepsin B involving the degradation of proteins and peptides contributes to diverse physiological processes such as protein processing, wound healing, apoptosis, inflammation, neurodegeneration, etc. [7,8]. Thus, overexpression of cathepsin B is associated with various pathological conditions such as a tumor, metastasis, migraine, angiogenesis, Alzheimer's disease, myocardial infarction, pancreatitis, etc. [9]. The diverse pathogenic functions associated with overexpression of cathepsin B make them a biomarker and therapeutic target for various diseases including cancer, neurodegenerative disorders such as Alzheimer's disease, rheumatoid arthritis, etc. and highlight the need for further potential research in the area of synthesis of novel drug candidates capable of inhibiting the cathepsin B enzyme.

Owing to their presence in >85 % of drugs, heterocycles are considered as imperative and privileged architectures for designing the newer drug candidates [10]. Especially, 1,2,3-triazoles and 1,3,4-oxadiazoles are significant biologically active heterocycles possessing diverse therapeutic effects encompassing antimicrobial, anti-inflammatory, anti-tumor, antiviral, antioxidant, etc. activities [11, 12]. Furthermore, the benzenesulfonamide motif has also been proven

* Corresponding author.
E-mail addresses: inssa.sitaram@gmail.com, sitaram@jcboseust.ac.in (S. Ram).
[1] The first two authors have contributed equally to this work.

https://doi.org/10.1016/j.molstruc.2024.139680
Received 25 June 2024; Received in revised form 1 August 2024; Accepted 15 August 2024
Available online 17 August 2024

to be as an amazing entity in the field of the development of potent biological agents. There are numerous reports in the literature exploring the fascinating profile of 1,2,3-triazoles, 1,3,4-oxadiazoles, and benzenesulfonamide as cathepsin B inhibitors. Siwach et al. [13] have reported carboxylic acid and ester functionalized 1,2,3-triazole derivatives **1** as potent inhibitors of cathepsin B showing inhibition at 10^{-7} M concentration (Fig. 1). Novel 1,2,3-triazole-aurone hybrids **2** have been reported by Saroha et al. [14,15] as an anti-cathepsin B agent possessing inhibition activity at 10^{-5} M concentration (Fig. 1). Garg et al. [16] have reported the novel 2,5-diaryl-1,3,4-oxadiazoles **3** as potent inhibitors of cathepsin B at 10^{-8} M concentration (Fig. 1). The area of developing anti-cathepsin B inhibitors having benzenesulfonamide in their skeleton is also under progress. Cyano-*N*-acyl-4-amino-benzenesulfonamides **4** have been reported by Abdoli et al. [17] as potent inhibitors of cathepsin B (Fig. 1). Recently, Vats et al. [18] have reported keto-bridged dual triazol-containing benzenesulfonamides **5** as potent anti-cathepsin B agents (Fig. 1). Kumar et al. [19] have also reported the synthesis of thiadiazole linked benzenesulfonamides **6–8** as potent anti-cathepsin B agents possessing 50 % inhibition at 10^{-7} M concentration (Fig. 1).

The above reports on the anti-cathepsin B potential of heterocyclic molecules having one or more of the 1,2,3-triazole, 1,3,4-oxadiazole, and benzenesulfonamide moieties in their skeleton suggest the hybridization of all of these three in a single molecule would be a prominent step toward the development of novel, more potent, and efficient cathepsin B inhibitors. To the best of our knowledge, no anti-cathepsin agent having 1,2,3-triazole, 1,3,4-oxadiazole, and benzenesulfonamide motifs in a single skeleton has been reported till now. Motivated by the fascinating profile of 1,2,3-triazoles, 1,3,4-oxadiazoles, and benzenesulfonamide coupled with our quest to develop better cathepsin B inhibitors, we have designed and synthesized a series of twenty-one novel hybrids containing 1,2,3-triazole, 1,3,4-oxadiazole, and benzenesulfonamide motifs **9–11a-g** and evaluated the anti-cathepsin activity of the synthesized target molecules (Fig. 2).

Molecular docking is a computational tool used to predict the binding interactions between the receptors/enzymes and the synthesized ligands [20]. It plays an important role in the identification of biologically potent compounds by predicting the estimated binding energies based on the complementarities of shape and electrostatics between the active site of the receptor and the various possible conformations of the ligands [21-23]. The interpretation of docking results provides the key binding interactions which further help in the optimization of structural features of the designed compounds for enhanced potential and selectivity against the target enzyme [24,25]. DFT is another widely adopted computational tool for understanding the structural characteristics of designed compounds by providing HOMO-LUMO energies as well as other global reactivity parameters including HOMO-LUMO energy gaps, electronegativities, ionization energies, electron affinities, etc. [26-28]. This also helps in understanding the charge distribution within the structures of the molecules which plays an important role in the prediction of interactions with the target enzymes [29,30]. Molecular docking was performed for the most potent compounds **9d-f** among the series against the cathepsin B enzyme to understand the binding interactions with the enzyme. ADMET parameters were also calculated for compounds **9d-f** to check their drug-likeness behavior. DFT calculations were carried out for all the newly synthesized twenty-one target compounds to find out the values of HOMO-LUMO energies as well as global reactivity parameters

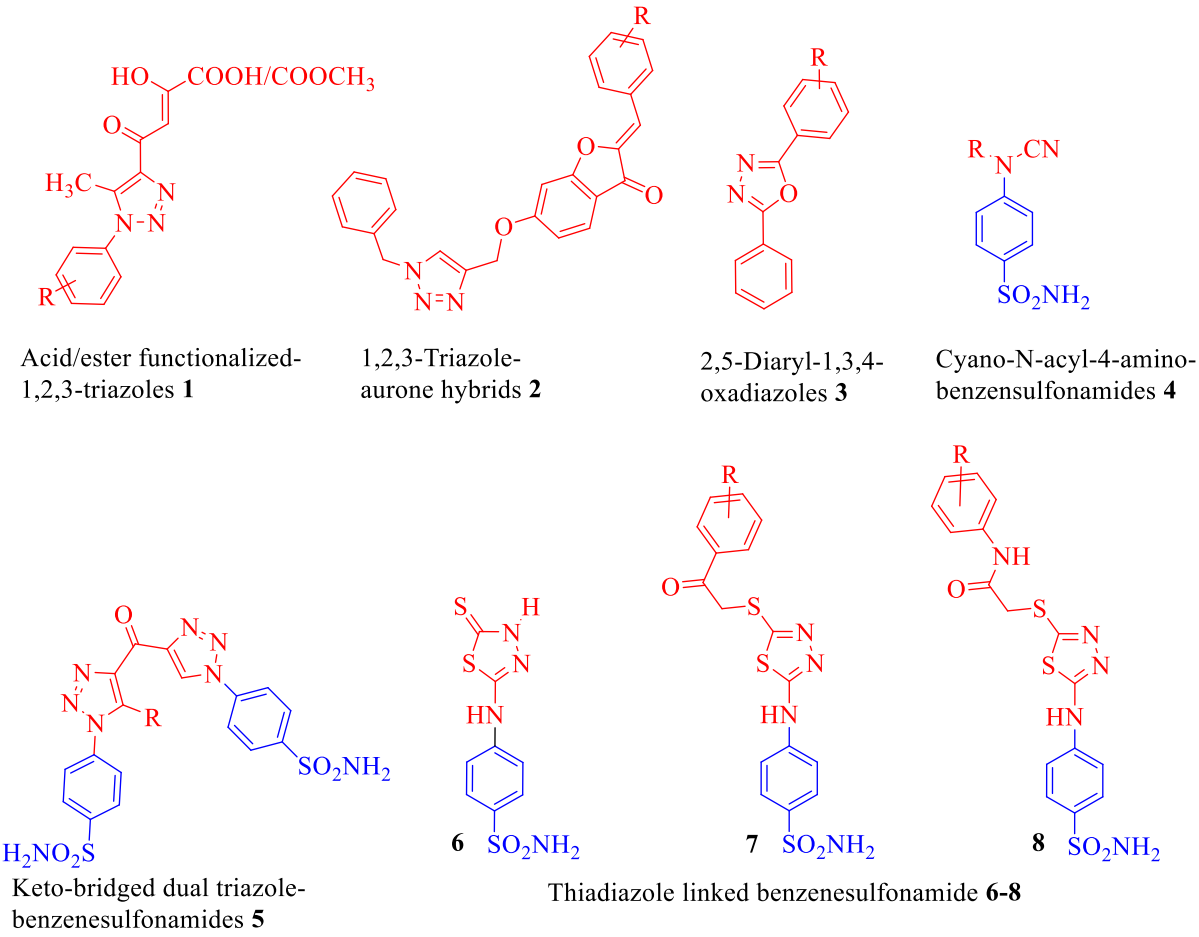

Fig. 1. Structures of the literature reported 1,2,3-triazole (1, 2, 5), 1,3,4-oxadiazole (3), and benzenesulfonamide (4–8) based anti-cathepsin B agents.

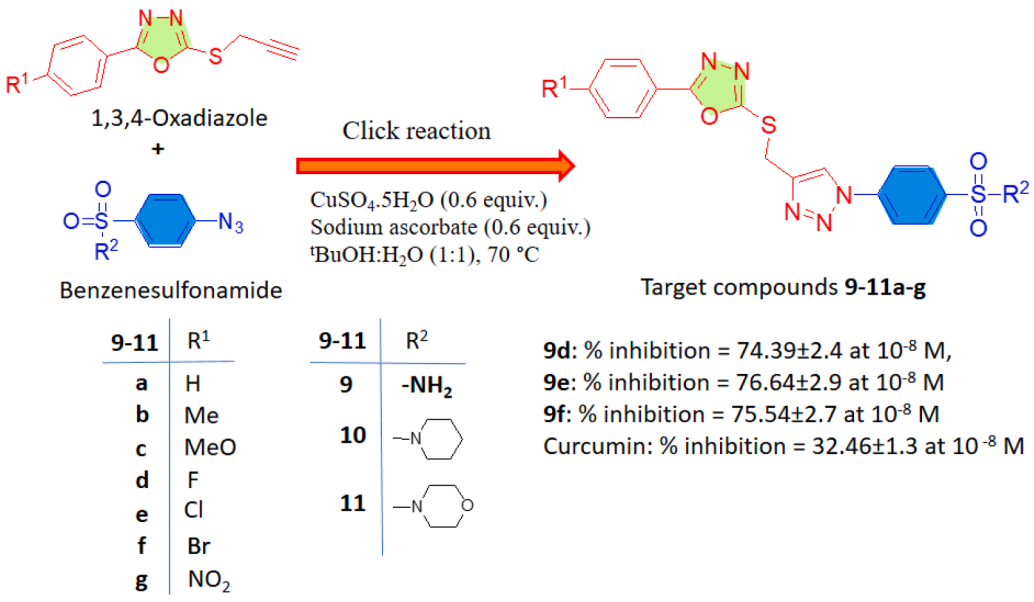

Fig. 2. Designing of the target compounds **9–11a-g** based on hybrid approach containing scaffolds triazole, oxadizaole, and benzenesulfonamide.

including electronegativity (χ), chemical potential (μ), chemical hardness (η), chemical softness (S), and electrophilicity index (ω).

2. Results and discussion

2.1. Synthesis

The procedure adopted for the synthesis of target compounds **9–11a-g** is depicted in scheme 1. Structures of all the hitherto unreported target compounds were confirmed by their spectral data (^{1}H NMR, ^{13}C NMR, and IR) and HRMS data.

Key intermediates for the synthesis of target compounds **9–11** were S-propargylated 1,3,4-oxadiazoles **15**, which were synthesized using the procedure reported in the literature by Alam et al. [31]. The synthesis starts with the esterification of 4-substituted benzoic acids **12** in the presence of conc. H_2SO_4 as a catalyst in methanol solvent followed by the treatment of the corresponding methyl benzoates with hydrazine monohydrate under refluxing conditions resulting in the formation of corresponding aryl hydrazides **13**. Further, the treatment of aryl hydrazides **13** under stirring conditions with carbon disulfide in DMF solvent at room temperature for 1 h followed by refluxing for 2–3 hrs resulted into the formation of 3-mercapto-1,3,4-oxadiazoles **14**. Propargylation of **14** using propargyl bromide in the presence of triethylamine as base yielded S-propargylated 1,3,4-oxadiazoles **15** which were further utilized as key intermediates for the synthesis of target compounds. Once having **15** in hand, target compounds **9/10/11** were

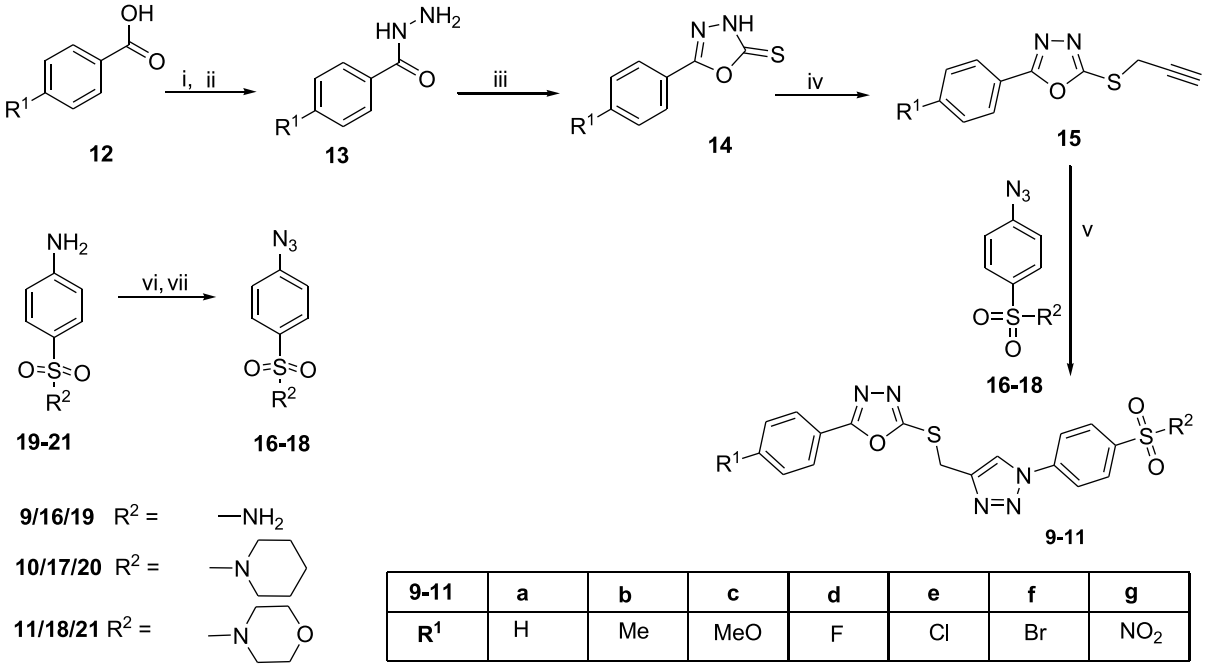

9-11	a	b	c	d	e	f	g
R^1	H	Me	MeO	F	Cl	Br	NO_2

Scheme 1. Synthesis of target compounds **9–11a-g**. Reagents and conditions: (i) Methanol, conc. H_2SO_4, reflux; (ii) Hydrazine hydrate, methanol, reflux; (iii) DMF, CS_2, reflux; (iv) Propargyl bromide, TEA, anhyd. ethanol, reflux; (v) $CuSO_4$·$5H_2O$, Sodium ascorbate, ^{t}BuOH:H_2O (1:1), 70 °C; (vi) $NaNO_2$/HCl, H_2O, 0 °C; (vii) NaN_3, H_2O, 0 °C.

obtained by click reactions of **15** with different sulfonamide substituted aryl azides **16/17/18**, respectively, in the presence of copper sulfate pentahydrate and sodium ascorbate. Aryl azides **16/17/18** used here were synthesized from 4-aminobenzenesulfonamide **19/20/21**, respectively, *via* the formation of corresponding diazonium salt using methodology reported by Batra et al. [32]. Further, the conversion of intermediate **15** into the desired target compounds **9–11** was confirmed by rigorous analysis of spectral data. In ^{1}H NMR, compounds **9–11** exhibited a singlet for two methylene protons (-SCH_2-) at approximately 4.75 ppm and another singlet at approximately 8.95 ppm for one proton of triazole ring confirming the formation of the desired products. In ^{13}C NMR, the methylene carbon atom (-SCH_2-) resonated at approximately 26 ppm while the methine carbon atom of the triazole ring (=CH-) resonated at approximately 162 ppm. The disappearance of a sharp band in the range of 3350–3250 cm^{-1} corresponding to the ≡C—H stretch of the terminal alkyne group and another band at approximately 2150 cm^{-1} corresponding to -C≡C- stretch along with the appearance of two bands at approximately 1310 and 1150 cm^{-1} corresponding to asymmetric and symmetric $S = O$ stretches of sulfonamide group, respectively, supported the achievement of products. Further, HMRS data were also in full agreement with the formation of desired products.

2.2. Anti-cathepsin b activity

2.2.1. In-vitro evaluation

All the synthesized novel target compounds **9–11a-g** were investigated for their inhibition potential against cathepsin B enzyme using curcumin as a reference [33]. The findings of our *in-vitro* investigations are represented in Table 1 and the pictorial representation of results is given in Fig. 3. The graphs of log(concentration) vs. residual activity (%) for all the tested compounds are provided in the supporting information file (Table 2). Results reveal that all the synthesized compounds here show effective inhibition profiles for cathepsin B at very low concentrations (10^{-8} M). Furthermore, the results were compared with those of the cathepsin B inhibition studies of literature-reported triazoles [12] and benzenesulfonamide-based heterocyclic molecules [19] which also indicate that the compounds **9–11a-g** are comparatively potent inhibitors of cathepsin B.

Inhibition data of the compounds **9–11a-g** led us to the following insights regarding cathepsin B inhibitory properties along with the structure-activity relationships:

i. All the tested twenty-one target compounds **9–11a-g** exhibited excellent inhibition potential against cathepsin B enzyme at a very low concentration of 10^{-8} M. Inhibition potential exhibited by the investigated compounds is in the range of 42.50 – 76.64 % which is better than curcumin (taken as reference) showing 32.46 % inhibition potential.

ii. Comparison of cathepsin B inhibition activity of compounds of series **9** and **10** let us conclude that compounds of series **9** having a benzenesulfonamide moiety at 1-position of the 1,2,3-triazole ring were found to possess overall higher inhibition potential than the respective analogues in series **10** (having S-piperidyl substituted benzenesulfonamide). However, in case of comparison of series **9** and **11** (having S-morpholinyl substituted benzenesulfonamide), the compounds of series **9** with H (**9a**) and halogen atoms (**9d-f**) as substituents were found to have higher inhibition potential than their respective analogues in the series **11**, while the compounds with Me (**9b**), MeO (**9c**), and NO_2 (9 g) groups as substituents were found to have lower inhibition potential than their respective analogues in the series **11**. These findings suggest that the substitutions on the nitrogen atom of the sulfonamide group have a remarkable influence on the anti-cathepsin B activity of the compounds. This observation also confirms the pharmacophoric action of the sulfonamide motif for the cathepsin B inhibition activity of the target compounds.

Table 1
% Inhibition of cathepsin B at 10^{-8} M concentration and the IC_{50} values of the target compounds **9–11a-g**.

Compound	R^1	R^2	% Inhibition (10^{-8} M)	$IC_{50} \pm S.D.$
9a	H	-NH_2	59.48±1.3.7	$5.24 \times 10^{-9} \pm 1.4$
9b	Me	-NH_2	61.89±2.9	$4.46 \times 10^{-9} \pm 2.1$
9c	MeO	-NH_2	62.48±2.3	$4.07 \times 10^{-9} \pm 3.1$
9d	F	-NH_2	74.39±2.4	$2.81 \times 10^{-9} \pm 3.2$
9e	Cl	-NH_2	76.64±2.9	$2.51 \times 10^{-9} \pm 2.5$
9f	Br	-NH_2	75.54±2.7	$2.63 \times 10^{-9} \pm 2.8$
9g	NO_2	-NH_2	45.28±3.4	$1.99 \times 10^{-8} \pm 2.1$
10a	H		46.89±3.6	$2.23 \times 10^{-8} \pm 2.4$
10b	Me		52.48±3.3	$1.58 \times 10^{-8} \pm 1.9$
10c	MeO		56.42±3.6	$1.25 \times 10^{-8} \pm 1.5$
10d	F		49.52±3.3	$1.51 \times 10^{-8} \pm 2.1$
10e	Cl		48.28±3.6	$1.90 \times 10^{-8} \pm 1.9$
10f	Br		51.54±2.4	$7.94 \times 10^{-9} \pm 1.3$
10g	NO_2		41.54±3.8	$5.62 \times 10^{-8} \pm 1.4$
11a	H		40.58±3.3	$6.30 \times 10^{-8} \pm 3.2$
11b	Me		65.18±3.1	$3.98 \times 10^{-9} \pm 2.8$
11c	MeO		67.28±3.6	$3.71 \times 10^{-9} \pm 2.5$
11d	F		57.08±3.5	$5.12 \times 10^{-9} \pm 2.3$
11e	Cl		42.5 ± 2.2	$3.98 \times 10^{-8} \pm 1.3$
11f	Br		44.68±2.8	$3.16 \times 10^{-8} \pm 1.7$
11g	NO_2		60.79±1.8	$5.01 \times 10^{-9} \pm 2.3$
Curcumin	–	–	32.46±1.3	$3.98 \times 10^{-8} \pm 2.5$

iii. Among all the compounds of series **9, 10**, and **11**, the compounds having substitution as H (a neutral substituent) have exhibited the lowest inhibition activity within their respective series except for the compounds 9 g and 10 g. This observation helps us to conclude that the substitution with both the electron-donating as well as electron-withdrawing groups has a positive influence on the anti-cathepsin B activity of the investigated compounds.

iv. In the case of the compounds of series **9**, the presence of an electron-withdrawing group as a substituent has exerted a stronger enhancing influence on the cathepsin B inhibition activity than the electron-donating groups. However, this observation was not true for the compounds of series **10** and **11**. In

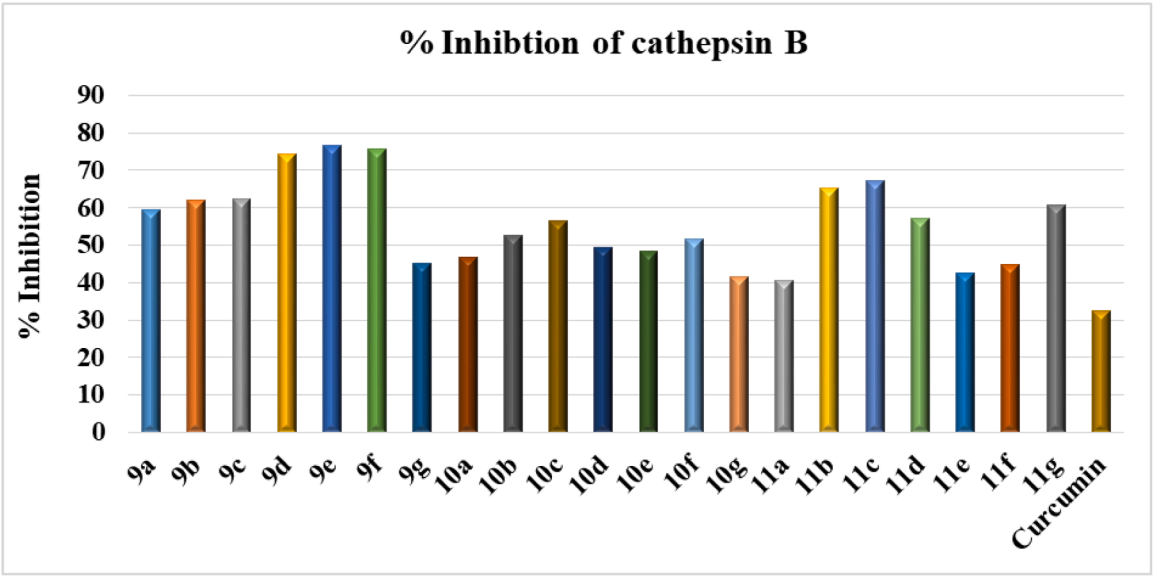

Fig. 3. % Inhibition of cathepsin B enzyme by the compounds **9–11a-g**.

particular, compounds of series **10** and **11** having halogen substitutions were found to be comparatively weaker inhibitors than their corresponding methyl and methoxy analogues.

v. Compound **9e** (having chloro group) was found to possess the highest inhibition potential among the synthesized series of compounds with 76.64 % inhibition at 10^{-8} M concentration followed by the compounds **9f** (having bromo substitution) and **9d** (having fluoro substitution) with 75.54 % and 74.39 % inhibition values, respectively.

2.2.2. *Molecular docking*

Molecular docking is a very well-known computational tool for understanding the interactions between receptors such as enzymes, proteins, DNA, RNA, etc., and the ligands, either natural or synthetic molecules [34]. It virtually predicts the best binding conformations of ligands for the complex formation with the enzyme in terms of binding energies, inhibition constants, intermolecular energies, etc. We have performed the molecular docking simulation of the most active anti-cathepsin B compounds **9d-f** against the cathepsin B enzyme. The PDB ID: 1GMY crystal structure was used for molecular docking as it provides a high-quality detailed view of the active site of cathepsin B having a resolution of 1.90 Å, which is considered a good resolution for accurate representation of the atomic orbitals of the enzyme [35]. The higher value of free energy of binding means better binding between the ligand and the enzyme [28-30]. The binding energies obtained for compounds **9d, 9e, 9f**, and curcumin in the active site of cathepsin B enzyme are −7.64 kcal/mol, −9.48 kcal/mol, −8.18 kcal/mol, and −4.82 kcal/mol, respectively. The highest value of free energy of

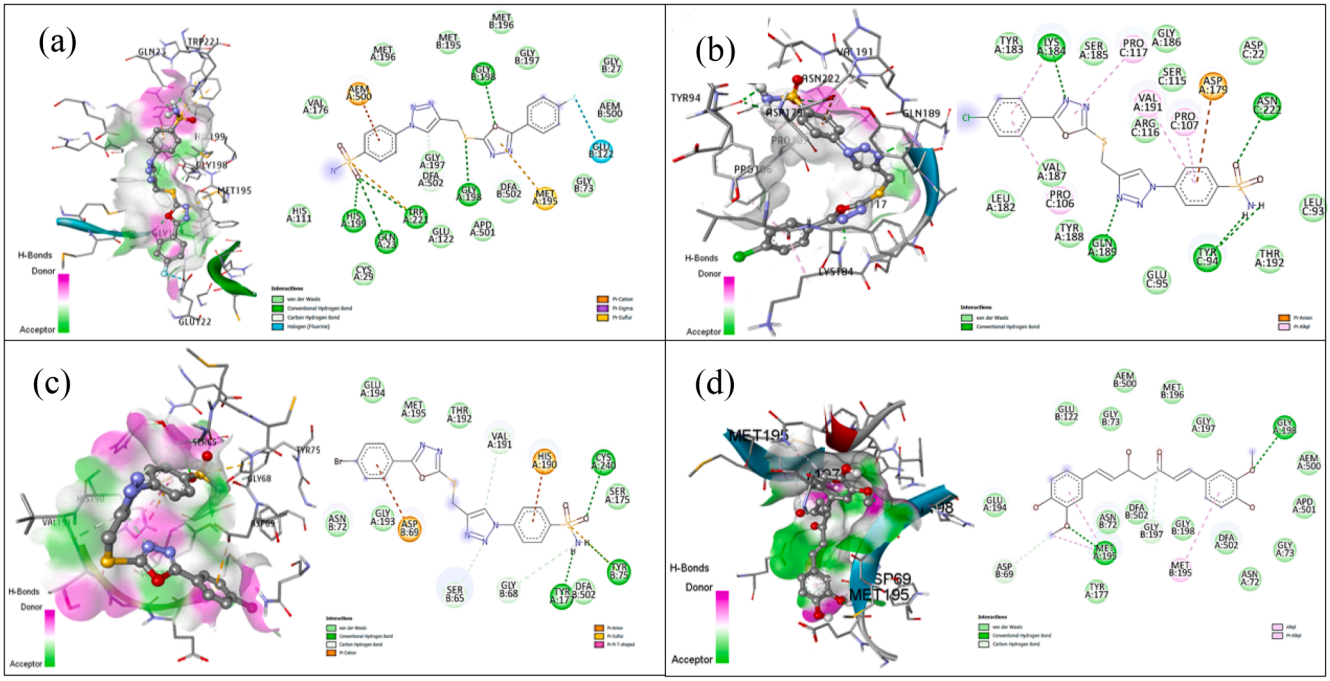

Fig. 4. (a) Pictorial representation of ligand **9d** with cathepsin B enzyme, (b) pictorial representation of ligand **9e** with cathepsin B enzyme,(c) pictorial representation of ligand **9f** with cathepsin B enzyme, (d) pictorial representation of curcumin with cathepsin B enzyme.

binding of **9e** with the cathepsin B enzyme is in line with the experimentally obtained highest inhibition activity of **9e**, among the three docked ones, against the cathepsin B enzyme.

Compound **9d** interacts with the target enzyme by the formation of five conventional hydrogen bonds with the HIS A:99, GLN A:23, TRP A:221, GLY A:198, and GLY B:198 amino acid residues (Fig. 4a). Additionally, formation of one pi-sulfur bond with TRP A:221, two pi-cation bonds with AEM A:500 and MET A:195, and one halogen (fluorine) bond with GLU B:122 was also observed. Compound **9e** interacts in the active site of cathepsin B enzyme with the formation of four conventional hydrogen bonds with three amino acid residues namely LYS A:184, GLN A:189, and TYR C:94. Along with these hydrogen bonds, four pi-alkyl interactions with LYS A:184, PRO C:117, PRO C:106, VAL A:191, and PRO C:107 amino acid residues as well as one pi-anion interaction with ASP A:179 amino acid residue were also formed in the enzyme-inhibitor complex (Fig. 4b). In case of compound **9f**, three hydrogen bonds with CYS A:240, TYR A:177, TYR B:75 amino acid residues and three van der Waals bonds with VAL A:191, SER B:65, and GLY B:68 amino acid residues were observed in the docked complex with cathepsin B enzyme (Fig. 4c). Further, from the results of docking study of curcumin against cathepsin B enzyme, we observed that curcumin interacts with the target enzyme by the formation of two conventional hydrogen bonds with MET A:195 and GLY A:198 amino acid residues (Fig. 4d). One van der Walls bond, two pi-alkyl bonds, and one alkyl bond were also formed in the complex of curcumin and the target enzyme. As from the interactions of co-crystallized ligand in the active site of 1GMY (provided at RCSB protein data bank), we have observed that the co-crystallized ligand interacts with the cathepsin B enzyme (PDB ID: 1GMY) by the formation of three conventional hydrogen bonds i.e. one with the oxygen of GLY A:74, one with the nitrogen of GLY A:74, and one with the nitrogen of GLY A:198 amino acid residues. Comparison of the interactions of compound **9d** with the interactions of co-crystallized ligand led us to conclude that both compound **9d** and co-crystallized ligand interact with GLY A:198 amino acid residue through hydrogen bond formation. Curcumin has also been found to possess one common interaction with the co-crystallized ligand in the active site of enzyme i.e. hydrogen bond interaction with GLY A:198 amino acid residue. However, no such common interaction could be observed in the case of compounds **9e** and **9f**.

It can be clearly seen from the results obtained that the sulfonamide group of the synthesized target compounds is involved in their inhibitory action against cathepsin B with the formation of three hydrogen bonds and one pi-sulfur bond in case of compound **3d**, three conventional hydrogen bonds in case of compound **3e**, and three conventional hydrogen bonds along with one van der Walls bond in case of compound **3f**. This observation was in line with the inference drawn from experimental results regarding the pharmacophoric action of the benzenesulfonamide group in cathepsin B inhibition activity.

2.2.3. ADMET parameters

ADMET study is one of the most important parts of computational drug designing. It helps to predict the deposition of the drug inside the body and its adverse side effects. Pharmacokinetics of the most active anti-cathepsin B compounds **9d-f** was assessed by the study of ADMET (absorption, distribution, metabolism, excretion, and toxicity) parameters (Table 3, supplementary information file). According to Lipinski's rule, an orally administrative drug molecule should fulfil the following conditions: no. of hydrogen bond donors <5, no. of hydrogen bond acceptors <10, molecular weight <500, logP (partition coefficient) <5, mol. refractivity = 40–130, and TPSA (topological polar surface area) <140 Å. A molecule will unlikely behave as an orally administrative drug if it violates any two or more than two of the conditions of Lipinski's rule. The values of ADMET parameters were calculated for the most potent anti-cathepsin B agents **9d-f** and the results are given in Table 2 (supplementary information file). Compounds **9d-f** were found to live up to all the parameters of Lipinski's rule within the acceptable range suggesting good drug likeness behaviour of them as orally administered drugs.

2.3. DFT calculations

Values of global reactivity descriptors convey important information about the chemical reactivity of the compounds. Using the energies of FMOs, values of various global reactivity parameters including HOMO-LUMO energy gap (ΔE_g), chemical hardness (η), chemical softness (S), chemical potential (μ), electronegativity (χ), and electrophilicity index (ω) were calculated for all the target compounds. The results obtained are depicted in Table 4 (supplementary information file). A smaller value of the HOMO-LUMO energy gap, lower hardness, and higher softness may be attributed to the higher reactivity of the molecules [36]. The compounds of series **10** (except 10 g) have lower values of energy gap, lower values of chemical hardness, and higher values of chemical softness than their counterparts in series **11** which in turn have lower values of energy gap, lower values of chemical hardness and higher values of chemical softness than their counterparts in series **9**. These results suggest that the compounds of series **10** (except the nitro derivatives) are more reactive than their respective analogues in series **11** followed by their respective analogues in series **9**. In the case of nitro derivatives, compound 9 g should be more reactive than compound 10 g followed by compound 11 g as per the values obtained. Nitro derivatives have the lowest values of ΔE_g within their respective series (9 g [NO_2] < **9e** [Cl] = **9d** [F] < **9f** [Br] < **9a** [H] < **9c** [MeO] < **9b** [Me], 10 g [NO_2] < **10e** [Cl] < **10d** [F] < **10f** [Br] < **10a** [H] < **10b** [Me] < **10c** [MeO], and 11 g [NO_2] < **11f** [Br] < **11e** [Cl] < **11d** [F] < **11a** [H] < **11b** [Me] < **11c** [MeO]). Further, they have the lowest values of chemical hardness and the highest values of chemical softness. These results suggest that the nitro derivatives are the most reactive ones within their respective series. Further, the lower value of E_{LUMO} suggests the more stable LUMO and the higher electron acceptance ability of the compound. The LUMOs of the compounds of series **9** have lower energy and thus are more stable than their respective analogues in series **10** which in turn are more stable than their respective analogues in series **11**. From this, we can conclude that compounds of series **9** are better electron acceptors than their respective analogues in series **10**, which are better electron acceptors than their counterparts in series **11**. It is noteworthy here that the compounds of series **9** are overall better anti-cathepsin B agents also in comparison to the compounds of series **10** and **11**, suggesting that the electron acceptance power could be considered as one of the important factors in determining the cathepsin B inhibition potential of the compounds.

3. Conclusion

Herein, we have reported the synthesis of a library of novel hybrids containing 1,2,3-triazole, 1,3,4-oxadiazole, and benzenesulfonamide motifs using a molecular hybridization approach. Further, all the target compounds were well characterized by rigorous analysis of their spectral (^{1}H, ^{13}C NMR, IR) and HRMS data. *In-vitro* evaluation of all the newly synthesized compounds was performed against cathepsin B enzyme, a biomarker and therapeutic target for several diseases. All the investigated hybrids were found to possess excellent inhibitory potential with 40.50 −76.64 % inhibition at 10^{-8} M concentrations as compared to the reference, curcumin (% inhibition = 32.46 % at 10^{-8} M concentration). Findings of the SAR studies suggested the remarkable influence of substitutions on the nitrogen atom of the sulfonamide group and compounds **9d-f** were found to exhibit the highest cathepsin B inhibition activity. ADMET calculations further proved the most active hybrids **9d-f** as safer drug candidates in terms of Lipinski's rule of five. Results of DFT calculations suggested the compounds of series **9** to be better electron acceptors than their respective counterparts in the series **10** followed by their respective counterparts in series **11**. As a conclusive remark, we can say that even though 1,2,3-triazoles, 1,3,4-oxadiazoles,

and benzenesulfonamides have already been individually developed as potent inhibitors of cathepsin B enzyme, herein, hybrids of these three motifs have been successfully explored as excellent anti-cathepsin B agents for the first time.

4. Experimental

4.1. General information

All chemicals were purchased from Spectrochem and Merck chemical companies. TLC (Thin layer chromatography) was carried out on silica-aluminum plates using long-range ultraviolet chamber for visualization of TLC plates. All glasswares' were used after drying in an oven for 12 hrs. Open capillaries were used to determine melting points in the digital melting point apparatus and are thus found uncorrected. Infrared (IR) spectra were recorded on the Perkin Elmer Spectrophotometer. ^{1}H and ^{13}C NMR data were recorded on Bruker Advance Neo 500 MHz NMR Spectrometer and JNM-ECZ 400S: 400 MHz NMR Spectrometer in pure DMSO-d_6 using TMS (Tetramethylsilane) as internal reference. HRMS (High-resolution mass spectrum) data were recorded on SYNAPT-XS#DBA064 in ESI (Electron spray ionization) modes. The reference values for the residual solvent were taken as δ = 2.50 ppm (DMSO-d_6) for ^{1}H NMR, δ = 39.54 ppm (DMSO-d_6) for ^{13}C NMR. The abbreviations: *s* = singlet, *d* = doublet, dd doublet of doublets, *m* = multiplets, and ex = exchangeable protons are used for NMR assignments.

4.2. General method of synthesis of target compounds 9–11a-g

To well-stirred solution of aromatic azide **17**/**18**/**19** (1.0 equivalent) and S-propargylated 1,3,4-oxadiazole **16** (1.0 equivalents) in tert-butanol and water (1:1), a solution of sodium ascorbate (0.6 equivalent) in water (2 mL) was added. After 10 min, a solution of $CuSO_4{\cdot}5H_2O$ (0.6 equivalent) in water (2 mL) was added and the reaction mixture was allowed to stir at 70 °C for 6 hrs. Reaction progress was monitored using TLC. After completion of the reaction, the reaction mixture was poured over crushed ice. The solid obtained was filtered, dried, and then recrystallized from ethanol yielding the pure product **9**/**10**/**11**.

4-((4-Amino-5-phenyl-4H-1,2,4-triazol-3-yl)amino)benzenesulfonamide (9a)

Yield: 75 %; solid; m.p.:180–182 °C; IR (KBr,cm^{-1}):3342, 3260, 3030, 2975, 1311 & 1156; ^{1}H NMR (400 MHz, DMSO-d_6): δ = 8.92 (s, 1H, triazole H), 8.10 (d, *J* = 7.2 Hz, 2H, Ar), 8.05–7.90 (m, 5H, Ar), 7.59 (s, *J* = 7.2 Hz, 2H, Ar), 7.53 (s, 2H, SO_2NH_2), 4.75 (s, 2H, CH_2S); ^{13}C NMR (126 MHz, DMSO-d_6): δ = 165.45, 162.90, 144.04, 143.92, 138.46, 132.09, 129.45, 127.51, 126.44, 123.05, 122.37, 120.39, 26.70; HRMS (*m/z*): $[M + H]^+$ calcd for $C_{17}H_{14}N_6O_3S_2$: 415.0647: Found 415.0616.

4-(4-(((5-(p-Tolyl)−1,3,4-oxadiazol-2-yl)thio)methyl)−1H-1,2,3-triazol-1-yl)benzenesulfonamide (9b)

Yield: 76 %; solid; m.p.:228–230 °C; IR (KBr, cm^{-1}): 3334, 3356, 2982, 1312, 1154, 618; ^{1}H NMR (400 MHz, DMSO-d_6): δ = 8.93 (s, 1H, triazole H), 8.11 (d, 2H, *J* = 8.8 Hz, Ar), 8.01 (d, *J* = 8.8 Hz, 2H, Ar), 7.86 (d, *J* = 8.0 Hz, 2H, Ar), 7.54 (s, 2H, SO_2NH_2), 7.39 (d, *J* = 8.0 Hz, 2H, Ar), 4.75 (s, 2H, CH_2S), 2.39 (s, 3H, Me); ^{13}C NMR (126 MHz, DMSO-d_6): δ = 165.62, 162.59, 144.12, 143.97, 142.38, 138.52, 130.06, 127.59, 126.47, 122.42, 120.45, 120.34, 26.75, 21.20; HRMS (*m/z*): $[M + H]^+$ calcd for $C_{18}H_{16}N_6O_3S_2$: 429.0803: Found 429.0827.

4-(4-(((5-(4-Methoxyphenyl)−1,3,4-oxadiazol-2-yl)thio)methyl)−1H-1,2,3-triazol-1-yl)benzenesulfonamide (9c)

Yield: 82 %; solid; m.p.: 234–36 °C; IR (KBr, cm^{-1}):3336, 3354, 2984, 1314, 1150, 602; ^{1}H NMR (400 MHz, DMSO-d_6): δ = δ 8.89 (s, 1H, triazole H), 8.09 (d, *J* = 6.8 Hz, 2H, Ar), 7.99 (d, *J* = 6.8 Hz, 2H, Ar), 7.89` (d, *J* = 7.2 Hz, 2H, Ar), 7.51 (s, 2H, SO_2NH_2), 7.11 (d, *J* = 7.2 Hz, 2H, Ar), 4.72 (s, 2H, CH_2S), 3.83 (s, 3H, OMe); ^{13}C NMR (126 MHz, DMSO-d_6): δ = 165.31, 162.01, 161.93, 143.98, 143.82, 138.36, 128.24, 127.42, 122.24, 120.29, 115.31, 114.80, 55.46, 26.6; HRMS (*m/z*): $[M + H]^+$ calcd for $C_{18}H_{16}N_6O_4S_2$: 445.0752: Found 445.0791.

4-(4-(((5-(4-Fluorophenyl)−1,3,4-oxadiazol-2-yl)thio)methyl)−1H-1,2,3-triazol-1-yl)benzenesulfonamide (9d)

Yield: 78 %; solid; m.p.: 226–228 °C; IR (KBr, cm^{-1}): 3330, 3346, 2982, 1310, 1150; ^{1}H NMR (400 MHz, DMSO-d_6): δ = 8.93 (s, 1H, triazole H), 8.11 (d, 2H, *J* = 8.8 Hz, Ar), 8.05 (dd, $^3J_{H-H}$ = 8.8 Hz &$^4J_{H\text{-}F}$ = 5.6 Hz, 2H, Ar), 8.01 (d, *J* = 8.8 Hz, 2H, Ar), 7.53 (s, 2H, SO_2NH_2), 7.45 (t,$^3J_{H-H}$&$^3J_{H\text{-}F}$ = 8.8 Hz, 2H, Ar), 4.75 (s, 2H, CH_2S); ^{13}C NMR (101 MHz, DMSO-d_6): δ = 164.28 (d, $^1J_{C\text{-}F}$ = 184.83 Hz), 163.45, 163.39, 144.43, 138.97, 129.68 (d, $^3J_{C\text{-}F}$ = 9.09 Hz), 128.03, 122.89, 122.87, 120.88, 120.27 (d, $^4J_{C\text{-}F}$ = 4.04 Hz), 117.21 (d, $^2J_{C\text{-}F}$ = 22.22 Hz), 27.20; HRMS (*m/z*): $[M + H]^+$ calcd for $C_{17}H_{13}FN_6O_3S_2$: 433.0552: Found 433.0522.

4-(4-(((5-(4-Chlorophenyl)−1,3,4-oxadiazol-2-yl)thio)methyl)−1H-1,2,3-triazol-1-yl)benzenesulfonamide (9e)

Yield: 80 %; solid; m.p.: 232–234 °C; IR (KBr, cm^{-1}): 3336, 3342, 2980, 1314, 1154 ; ^{1}H NMR (400 MHz, DMSO-d_6) δ = 8.90 (s, 1H, triazole H), 8.09 (d, *J* = 7.2 Hz, 2H, Ar), 8.10 - 7.97 (m, 4H, Ar), 7.65 (d, *J* = 7.2 Hz, 2H, Ar), 7.53 (s, 2H, SO_2NH_2), 4.75 (s, 2H, CH_2S); ^{13}C NMR (126 MHz, DMSO-d_6): δ = 164.74, 163.27, 144.03, 143.98, 138.50, 136.86, 129.68, 128.32, 127.57, 122.41, 121.99, 120.45, 26.72;HRMS (*m/z*): $[M + H]^+$/$[M + H + 2]^+$calcd for$C_{17}H_{13}ClN_6O_3S_2$: 449.0257/451.0228: Found 449.0185/451.0167.

4-(4-(((5-(4-Bromophenyl)−1,3,4-oxadiazol-2-yl)thio)methyl)−1H-1,2,3-triazol-1-yl)benzenesulfonamide (9f)

Yield: 72 %; solid; m.p.: 240–242 °C; IR (KBr, cm^{-1}): 3331, 3352, 2972, 1313, 1154, 612; ^{1}H NMR (400 MHz, DMSO-d_6) δ = 8.91 (s, 1H, triazole H), 8.10 (d, *J* = 8.8 Hz, 2H, Ar), 8.00 (d, *J* = 8.8 Hz, 2H, Ar), 7.91 (d, *J* = 8.8 Hz, 2H, Ar), 7.80 (d, *J* = 8.8 Hz, 2H, Ar) 7.53 (s, 2H, SO_2NH_2), 4.76(s, 2H, CH_2S); ^{13}C NMR (126 MHz, DMSO-d_6): δ = 164.84, 163.27, 144.00, 143.97, 138.49, 132.58, 128.41, 127.55, 125.72, 122.40, 122.32, 120.44, 26.70;HRMS (*m/z*): $[M + H]^+$/$[M + H + 2]^+$calcd for $C_{17}H_{13}BrN_6O_3S_2$: 492.9752/494.9732: Found 492.9746/494.9742.

4-(4-(((5-(4-Nitrophenyl)−1,3,4-oxadiazol-2-yl)thio)methyl)−1H-1,2,3-triazol-1-yl)benzenesulfonamide (9 g)

Yield: 68 %; solid; m.p.: 245–247 °C; IR (KBr, cm^{-1}): 3331, 3353, 2981, 1314, 1154; ^{1}H NMR (400 MHz, DMSO-d_6): δ = 8.93 (s, 1H, triazole H), 8.40 (d, *J* = 8.4 Hz, 2H, Ar), 8.23 (d, *J* = 8.4 Hz, 2H, Ar), 8.10 (d, *J* = 8.0 Hz, 2H, Ar), 8.00 (d, *J* = 8.0 Hz, 2H, Ar), 7.53 (s, 2H, SO_2NH_2), 4.80 (s, 2H, CH_2S); ^{13}C NMR (126 MHz, DMSO-d_6): δ = 164.20, 163.90, 148.99, 143.75, 138.27, 128.39, 127.68, 127.63, 127.32, 124.44, 122.25, 120.21, 26.49; HRMS (*m/z*): $[M + H]^+$ calcd for $C_{17}H_{13}N_7O_5S_2$: 460.0497: Found 460.0523.

2-Phenyl-5-(((1-(4-(piperidin-1-ylsulfonyl)phenyl)−1H-1,2,3-triazol-4-yl)methyl)thio)−1,3,4-oxadiazole (10a)

Yield: 76 %; solid; m.p.: 241–243 °C; IR (KBr, cm^{-1}): 2980, 1314, 1153; ^{1}H NMR (400 MHz, DMSO-d_6): δ = 8.97 (s, 1H, triazole H), 8.16 (d, *J* = 8.4 Hz, 2H, Ar), 7.96 (d, *J* = 6.8 Hz, 2H, Ar), 7.91 (d, *J* = 8.4 Hz, 2H, Ar), 7.64–7.56 (m, 3H, Ar), 4.76 (s, 2H, CH_2S), 2.91 (s, 4H, CH_2N), 1.53 (s, 4H, CH_2), 1.34 (s, 2H, CH_2); ^{13}C NMR (126 MHz, DMSO-d_6): δ = 165.29, 162.71, 144.01, 139.19, 135.25, 131.92, 129.30, 129.20, 126.29, 122.91, 122.28, 120.41, 46.43, 26.56, 24.53, 22.64; HRMS (*m/z*): $[M + H]^+$ calcd for $C_{22}H_{22}N_6O_3S_2$: 483.1273: Found 483.1299.

2-(((1-(4-(Piperidin-1-ylsulfonyl)phenyl)−1H-1,2,3-triazol-4-yl) methyl)thio)−5-(p-tolyl)−1,3,4-oxadiazole (10b)

Yield: 80 %; solid; m.p.: 250–252 °C; IR (KBr, cm^{-1}): 2956, 1314, 1154; ^{1}H NMR (400 MHz, DMSO-d_6): δ = 8.97 (s, 1H, triazole H), 8.16 (d, *J* = 8.0 Hz, 2H, Ar), 7.92 (d, *J* = 8.0 Hz, 2H, Ar), 7.85 (d, *J* = 7.6 Hz, 2H, Ar), 7.38 (d, *J* = 7.6 Hz, 2H, Ar), 4.75 (s, 2H, CH_2S), 2.91 (s, 4H, CH_2N), 2.38 (s, 3H, CH_3), 1.53 (s, 4H, CH_2), 1.35 (s, 2H, CH_2); ^{13}C NMR (126 MHz, DMSO-d_6): δ = 165.41, 162.34, 144.06, 142.15, 139.20, 135.26, 129.85, 129.22, 126.27, 122.28, 120.43, 120.17, 46.44, 26.55, 24.54, 22.64, 21.00; HRMS (*m/z*): $[M + H]^+$ calcd for $C_{23}H_{24}N_6O_3S$: 497.1429: Found 497.1424.

2-(4-Methoxyphenyl)−5-(((1-(4-(piperidin-1-ylsulfonyl)phenyl)−1H-

1,2,3-triazol-4-yl)methyl)thio)−1,3,4-oxadiazole (10c)

Yield: 83 %; solid; m.p.: 256–258 °C; IR (KBr, cm^{-1}): 2965, 1312, 1153; ^{1}H NMR (300 MHz, DMSO-d_6): δ = 8.94 (s, 1H, triazole H), 8.15 (d, *J* = 8.7 Hz, 2H, Ar), 7.96–7.84 (m, 4H, Ar), 7.10 (d, *J* = 8.7 Hz, 2H, Ar), 4.72 (s, 2H, CH_2S), 3.82 (s, 3H, OCH_3), 2.91 (s, 4H, CH_2N), 1.53 (s, 4H, CH_2), 1.34 (s, 2H, CH_2); ^{13}C NMR (126 MHz, DMSO-d_6): δ = 165.27, 161.94, 161.90, 143.84, 139.24, 135.27, 129.07, 128.05, 122.00, 120.19, 115.27, 114.52, 55.27, 46.43, 26.52, 24.59, 22.75; HRMS (*m/z*): $[M + H]^+$ calcd for $C_{23}H_{24}N_6O_4S_2$: 513.1378: Found 513.1370.

2-(4-Fluorophenyl)−5-(((1-(4-(piperidin-1-ylsulfonyl)phenyl)−1H-1,2,3-triazol-4-yl)methyl)thio)−1,3,4-oxadiazole (10d)

Yield: 76 %; solid; m.p.: 246–248 °C; IR (KBr, cm^{-1}): 2962, 1315, 1150; ^{1}H NMR (400 MHz, DMSO-d_6): δ = 8.95 (s, 1H, triazole H), 8.13 (d, *J* = 8.8 Hz, 2H, Ar), 8.04–7.93 (m, 2H, Ar), 7.92 (d, *J* = 8.8 Hz, 2H, Ar), 7.41 (t, $^3J_{H—H}$&$^3J_{H\text{-}F}$ = 8.8 Hz, 2H, Ar), 4.74 (s, 2H, CH_2S), 2.88 (s, 4H, CH_2N), 1.50 (s, 4H, CH_2), 1.32 (s, 2H, CH_2); ^{13}C NMR (126 MHz, DMSO-d_6): δ = 164.04 (d, $^1J_{C\text{-}F}$ = 250.74 Hz), 164.61, 163.05, 162.79, 144.03, 139.22, 135.30, 129.26, 129.09 (d, $^3J_{C\text{-}F}$ = 10.08 Hz), 122.31, 120.47, 119.65 (d, $^4J_{C\text{-}F}$ = 3.78 Hz), 116.62 (d, $^2J_{C\text{-}F}$ = 22.69 Hz), 46.48, 26.60, 24.58, 22.68; HRMS (*m/z*): $[M + H]^+$ calcd for $C_{22}H_{21}FN_6O_3S_2$: 501.1178: Found 501.1154.

2-(4-Chlorophenyl)−5-(((1-(4-(piperidin-1-ylsulfonyl)phenyl)−1H-1,2,3-triazol-4-yl)methyl)thio)−1,3,4-oxadiazole (10e)

Yield: 78 %; solid; m.p.: 238–240 °C; IR (KBr, cm^{-1}): 2968, 1315, 1148; ^{1}H NMR (400 MHz, DMSO-d_6) δ = 8.93 (s, 1H, triazole H), 8.12 (d, *J* = 8.4 Hz, 2H, Ar), 7.94 (d, *J* = 8.0 Hz, 2H, Ar), 7.88 (d, *J* = 8.4 Hz, 2H, Ar), 7.62 (d, *J* = 7.6 Hz, 2H, Ar), 4.72 (s, 2H, CH_2S), 2.88 (s, 4H, CH_2N), 1.50 (s, 4H, CH_2), 1.31 (s, 2H, CH_2); ^{13}C NMR (126 MHz, DMSO-d_6): δ = 163.08, 158.56, 139.23, 136.71, 135.32, 129.54, 129.27, 128.17, 122.34, 121.84, 120.49, 46.49, 31.19, 26.58, 24.58, 22.69;HRMS (*m/z*): $[M + H]^+/[M + H + 2]^+$calcd for $C_{22}H_{21}ClN_6O_3S_2$: 517.0883/519.0854: Found 517.0853/519.0852.

2-(4-Bromophenyl)−5-(((1-(4-(piperidin-1-ylsulfonyl)phenyl)−1H-1,2,3-triazol-4-yl)methyl)thio)−1,3,4-oxadiazole (10f)

Yield: 69 %; solid; m.p.: 252–254 °C; IR (KBr, cm^{-1}): 2965, 1310, 1156; ^{1}H NMR (400 MHz, DMSO-d_6) δ = 8.93 (s, 1H, triazole H), 8.13 (d, *J* = 8.4 Hz, 2H, Ar), 7.88 (m, 4H, Ar), 7.76 (d, *J* = 8.0 Hz, 2H, Ar), 4.72 (s, 2H, CH_2S), 2.88 (s, 4H, CH_2N), 1.50 (s, 4H, CH_2), 1.32 (s, 2H, CH_2); ^{13}C NMR (126 MHz, DMSO-d_6): δ = 164.72, 162.84, 144.01, 135.31, 132.46, 129.26, 128.28, 125.59, 122.33, 122.18, 120.48, 46.48, 31.20, 26.58, 24.58, 22.68;HRMS (*m/z*): $[M + H]^+/[M + H + 2]^+$calcd for $C_{22}H_{21}BrN_6O_3S_2$: 561.03782/563.0358: Found 561.0407/563.0405.

2-(4-Nitrophenyl)−5-(((1-(4-(piperidin-1-ylsulfonyl)phenyl)−1H-1,2,3-triazol-4-yl)methyl)thio)−1,3,4-oxadiazole (10 g)

Yield: 64 %; solid; m.p.: 258–260 °C; IR (KBr, cm^{-1}): 2986, 1316, 1152; ^{1}H NMR (400 MHz, DMSO-d_6): δ = 8.99 (s, 1H, triazole H), 8.41 (d, *J* = 8.4 Hz, 2H, Ar), 8.24 (d, *J* = 8.4 Hz, 2H, Ar), 8.17 (d, *J* = 8.4 Hz, 2H, Ar), 7.92 (d, *J* = 8.4 Hz, 2H, Ar), 4.80 (s, 2H, CH_2S), 2.92 (s, 4H, CH_2N), 1.53 (s, 4H, CH_2), 1.23 (s, 2H, CH_2); ^{13}C NMR (126 MHz, DMSO-d_6): δ = 163.98, 162.79, 143.89, 132.14, 129.22, 127.68, 124.51, 122.34, 120.45, 116.11, 114.61, 46.43, 31.68, 26.55, 24.53, 22.64; HRMS (*m/z*): $[M + H]^+$ calcd for $C_{22}H_{21}N_7O_5S_2$: 528.1123: Found 528.1161.

4-((4-(4-(((5-Phenyl-1,3,4-oxadiazol-2-yl)thio)methyl)−1H-1,2,3-triazol-1-yl)phenyl)sulfonyl)morpholine (11a)

Yield: 75 %; solid; m.p.: 254–256 °C; IR (KBr, cm^{-1}): 2976, 1314, 1152; ^{1}H NMR (400 MHz, DMSO-d_6): 9.00 (s, 1H, triazole H), 8.21(d, *J* = 8.8 Hz, 2H, Ar), 7.97 (d, *J* = 8.0 Hz, 4H, Ar), 7.94 (d, *J* = 8.8 Hz, 2H, Ar), 7.66–7.54 (m, 3H, Ar), 4.77 (s, 2H, CH_2S), 3.64 (s, 4H, CH_2N), 2.91 (s, 4H, CH_2O); ^{13}C NMR (126 MHz, DMSO-d_6): δ = 165.34, 162.75, 144.09, 139.51, 134.16, 131.97, 129.51, 129.33, 126.33, 122.92, 122.35, 120.55, 65.18, 45.77, 26.60; HRMS (*m/z*): $[M + H]^+$ calcd for $C_{21}H_{20}N_6O_4S_2$: 485.10657: Found 485.1094.

4-((4-(4-(((5-(p-Tolyl)−1,3,4-oxadiazol-2-yl)thio)methyl)−1H-1,2,3-triazol-1-yl)phenyl)sulfonyl)morpholine (11b)

Yield: 81 %; solid; m.p.: 251–253 °C; IR (KBr, cm^{-1}): 2978, 1310, 1154; ^{1}H NMR (400 MHz, DMSO-d_6): δ = 8.98 (s, 1H, triazole H), 8.20 (d, *J* = 8.0 Hz, 2H, Ar), 7.93 (d, *J* = 8.0 Hz, 2H, Ar), 7.85 (d, *J* = 7.6 Hz, 2H, Ar), 7.38 (d, *J* = 7.6 Hz, 2H, Ar), 4.75 (s, 2H, CH_2S), 3.63 (s, 4H, CH_2O), 2.91 (s, 4H, CH_2N), 2.38 (s, 3H, Me); ^{13}C NMR (126 MHz, DMSO-d_6): δ = 165.43, 162.35, 144.09, 142.16, 139.50, 134.16, 129.86, 129.50, 126.28, 122.32, 120.53, 120.19, 65.17, 45.76, 26.58, 21.02; HRMS (*m/z*): $[M + H]^+$ calcd for $C_{22}H_{22}N_6O_4S_2$: 499.1222: Found 499.1190.

4-((4-(4-(((5-(4-Methoxyphenyl)−1,3,4-oxadiazol-2-yl)thio)methyl)−1H-1,2,3-triazol-1-yl)phenyl)sulfonyl)morpholine (11c)

Yield: 76 %; solid; m.p.: 255–257 °C; IR (KBr, cm^{-1}): 2984, 1317, 1156; ^{1}H NMR (300 MHz, DMSO-d_6): δ = 8.93 (s, 1H, triazole H), 8.17 (d, *J* = 8.4 Hz, 2H, Ar), 7.92 (d, 8.7 Hz, 2H, Ar), 7.88 (d, 8.7 Hz, 2H, Ar), 7.10 (d, *J* = 8.7 Hz, 2H, Ar), 4.72 (s, 2H, CH_2S), 3.82 (s, 3H, OMe), 3.59 (s, 4H, CH_2O), 2.90 (s, 4H, CH_2N); ^{13}C NMR (126 MHz, DMSO-d_6): δ = 165.32, 161.95, 143.82, 139.56, 134.22, 129.32, 128.03, 121.96, 120.27, 115.28, 115.24, 114.45, 65.30, 55.23, 45.66, 26.50; HRMS (*m/z*): $[M + H]^+$ calcd for $C_{22}H_{22}N_6O_5S_2$: 515.1171: Found 515.1213.

4-((4-(4-(((5-(4-Fluorophenyl)−1,3,4-oxadiazol-2-yl)thio)methyl)−1H-1,2,3-triazol-1-yl)phenyl)sulfonyl)morpholine (11d)

Yield: 82 %; solid; m.p.: 247–249 °C; IR (KBr, cm^{-1}): 2986, 1314, 1150; ^{1}H NMR (400 MHz, DMSO-d_6): δ = 8.98 (s, 1H, triazole H), 8.19 (d, *J* = 8.8 Hz, 2H, Ar), 8.03 (dd, $^3J_{H—H}$ = 8.8 Hz, $^4J_{H\text{-}F}$ = 5.2 Hz, 2H, Ar), 7.93 (d, *J* = 8.8 Hz, 2H, Ar), 7.43 (t, $^3J_{H—H}$&$^3J_{H\text{-}F}$ = 8.8 Hz, 2H, Ar), 4.76 (s, 2H, CH_2S), 3.63 (t, *J* = 4.4 Hz, 4H, CH_2O), 2.91 (t, *J* = 4.4 Hz, 4H, CH_2N); ^{13}C NMR (126 MHz, DMSO-d_6): δ = 164.57, 164.00 (d, $^1J_{C\text{-}F}$ = 250.74 Hz), 162.76, 144.03, 139.49, 134.16, 129.49, 129.05 (d, $^3J_{C\text{-}F}$ = 8.82 Hz), 122.32, 120.53, 119.64 (d, $^4J_{C\text{-}F}$ = 2.52 Hz), 116.58 (d, $^2J_{C\text{-}F}$ = 22.68 Hz), 65.16, 45.74, 26.56; HRMS (*m/z*): $[M + H]^+$ calcd for $C_{21}H_{19}FN_6O_4S_2$: 503.0971: Found 503.0999.

4-((4-(4-(((5-(4-Chlorophenyl)−1,3,4-oxadiazol-2-yl)thio)methyl)−1H-1,2,3-triazol-1-yl)phenyl)sulfonyl)morpholine (11e)

Yield: 77 %; solid; m.p.: 245–247 °C; IR (KBr, cm^{-1}): 2984, 1315, 1152; ^{1}H NMR (400 MHz, DMSO-d_6) δ = 8.95 (s, 1H, triazole H), 8.16 (d, *J* = 8.4 Hz, 2H, Ar), 7.94 (d, *J* = 8.4 Hz, 2H, Ar), 7.90 (s, *J* = 8.4 Hz, 2H, Ar), 7.62 (d, *J* = 8.4 Hz, 2H, Ar), 4.75 (s, 2H, CH_2S), 3.59 (s, 4H, CH_2O), 2.87 (s, 4H, CH_2N); ^{13}C NMR (126 MHz, DMSO-d_6): δ = 164.59, 163.06, 144.04, 139.50, 136.69, 134.18, 129.65, 129.51, 128.15, 122.35, 121.84, 120.56, 65.18, 45.76, 26.56;HRMS (*m/z*): $[M+H]^+/[M + H + 2]^+$calcd for $C_{21}H_{19}ClN_6O_4S_2$: 519.0676/521.0646: Found 519.0692/521.0648.

4-((4-(4-(((5-(4-Bromophenyl)−1,3,4-oxadiazol-2-yl)thio)methyl)−1H-1,2,3-triazol-1-yl)phenyl)sulfonyl)morpholine (11f)

Yield: 75 %; solid; m.p.: 254–256 °C; IR (KBr, cm^{-1}): 2986, 1314, 1152; ^{1}H NMR (400 MHz, DMSO-d_6) δ = 8.99 (s, 1H, triazole H), 8.20 (d, *J* = 8.4 Hz, 2H, Ar), 7.94 (d, *J* = 8.4 Hz, 2H, Ar), 7.91 (d, *J* = 8.4 Hz, 2H, Ar), 7.80 (d, *J* = 8.4 Hz, 2H, Ar), 4.77 (s, 2H, CH_2S), 3.64 (s, 4H, CH_2O), 2.91 (s, 4H, CH_2N); ^{13}C NMR (126 MHz, DMSO-d_6): δ = 164.71, 163.10, 144.04, 139.51, 134.20, 132.45, 129.53, 128.28, 125.59, 122.36, 122.19, 120.58, 65.20, 45.78, 26.57;HRMS (*m/z*): $[M+H]^+/[M + H + 2]^+$calcd for $C_{21}H_{19}BrN_6O_4S_2$: 563.0170/565.0150: Found 563.0155/565.0187.

4-((4-(4-(((5-(4-Nitrophenyl)−1,3,4-oxadiazol-2-yl)thio)methyl)−1H-1,2,3-triazol-1-yl)phenyl)sulfonyl)morpholine (11 g)

Yield: 65 %; solid; m.p.: 243–245 °C; IR (KBr, cm^{-1}): 2976, 1314, 1154; ^{1}H NMR (400 MHz, DMSO-d_6): δ = 9.00 (s, 1H, triazole H), 8.41 (d, *J* = 8.4 Hz, 2H, Ar), 8.24 (d, *J* = 8.4 Hz, 2H, Ar), 8.20 (d, *J* = 8.4 Hz, 2H, Ar), 7.94 (d, *J* = 8.4 Hz, 2H, Ar), 4.81 (s, 2H, CH_2S), 3.63 (s, 4H, CH_2O), 2.91 (s, 4H, CH_2N); ^{13}C NMR (126 MHz, DMSO-d_6): δ = 164.21, 164.00, 149.10, 143.94, 139.49, 134.19, 129.50, 128.47, 127.70, 124.52, 122.39, 120.55, 65.16, 45.75, 26.56; HRMS (*m/z*): $[M + H]^+$ calcd for $C_{21}H_{19}N_7O_6S_2$: 530.0916: Found 530.0886.

4.3. Anti-cathepsin assay

Cathepsin B was purified by the standard protocol used [37].

Cathepsin B activity was assessed by incubating synthesized compounds with the enzyme in a phosphate buffer at pH 6.0 for 30 min. Stock solutions of the synthesized compounds were prepared at a concentration of 1 mM in DMSO and diluted with DMSO to achieve working standards ranging from 10^{-3} to 10^{-7} M. These were then incubated in 1.740 ml of 0.1 M phosphate buffer of pH 6.0 containing 2 mM thiol activator and approximately 1 mM EDTA for about 10 min at 37 °C. The effective concentration of the inhibitory compounds was calculated to be between 10^{-5} and 10^{-9} M. Thereafter, about, 20 μl of the prepared stock solutions in DMSO was added to the reaction mixture and incubated again at 37 °C for half an hour. Afterward, 40 μl of 40 mg BANA/ml DMSO was added as the substrate. The corresponding effective concentrations to the above working standards of the inhibitory compounds became between 10^{-5} and 10^{-9} M. The remaining enzyme activity was determined by adding Fast Garnet GBC solution, and the colorimetric quantification of the released β-naphthylamine was measured at 520 nm using a standard assay procedure. The results were compared to a control containing an equal amount of DMSO without any compound. The inhibition was studied with reference to curcumin, a known cathepsin B inhibitor [38,39].% Inhibition was calculated using the following formulas:% Inhibition= $[(A_C\text{-}A_S)/A_C)] \times 100$, where A_C and A_S represent the absorbance of the control and sample, respectively. The experiments were performed in triplicates and average values are reported in the following section.

4.4. Molecular docking

4.4.1. Protein and ligand file preparation

Ligand files were prepared minimized in energy using ChemDraw 3D and saved as .mol files. Open Babel was used to convert ligand mol files to pdb files. The cathepsin B protein pdb file was downloaded from the RCSB Protein data bank (https://www.rcsb.org/structure/1GMY) and prepared for docking by deleting water molecules, adding polar hydrogens, and adding Kollman charges to the protein in AutoDock 4.2 [40] and saved in pdbqt format. Ligand files were also converted to the pdbqt format required for molecular docking using AutoDock 4.2.

4.4.2. Grid box generation

Protein and ligand pdbqt files were opened in AutoDock 4.2. In the next step, grid box was generated keeping the dimensions in such a way that it covers the complete binding site of the protein. Saved the grid box parameter files as .gpf file after grid box generation and ran the autogrid4 application giving the output in .glg format.

4.4.3. Docking

Choose the macromolecule by setting the rigid file name and then open the ligand pdbqt file. Genetic algorithm with ten runs, 150 population size, maximum number of evals: medium-25,00,000, and keeping other parameters as default was used as search parameter. The docking parameter file was saved as Lamarckian GA4.2 in .dpf format. Ran the autodock4 application resulting in the docked output file in .dlg format [41,42].

4.4.4. Analysis of results and visualization

Opened the docking output (.dlg) file in AutoDock 4.2. Choose the macromolecule and play the conformation obtained ranked by energy. The highest binding energy conformation is selected as output and saved as a pdbqt file. Converted the output format from pdbqt to pdb. Discovery studio visualizer was used to open the output file, and 3D and 2D representations of output are reported in the manuscript.

4.4.5. Validation of docking protocol

For validation of docking protocol, we have performed docking of a co-crystallized ligand (N-cyanomethyl-Nα-(diphenylacetyl)−3-methyl-phenyl-alaninamide) into the original binding site of the protein structure 1GMY using the same protocol as used for the docking of most potent compounds **9d, 9e, 9f**, and curcumin and compared the results with available data of co-crystallized ligand [43]. Visual inspection of the result obtained from the molecular docking confirmed that key interactions of ligand and protein were same in protein-ligand docked complex and co-crystallized ligand complex. The consistency between the docking data and the crystallization data of the interactions of the ligand with the enzyme supports the acceptable reliability of our docking protocol in predicting ligand-binding interactions. The RMSD value of binding pose of the docked ligand and the co-crystallized ligand was found to be 0.899, which is also supports the accuracy of our docking protocol.

4.5. AMDET calculations

The ADMET parameters for most active compounds **9d-f** were calculated using an online ADME calculator at atomistic.online platform [44].

4.6. DFT calculations

We have prepared the structures of compounds in ChemDraw 8.0. The energy of compounds was minimized using ChemDraw 3D software with minimum RMS gradient: 0.100 and generated the gaussian input files using job type: compute properties. B3LYP method was used with closed shell (restricted) wavefunction. Basis set: 3–21 G was used with d polarization and keeping charges equals to zero and multiplicity equals to 1 using gas phase solvation model. Now the files were saved in Gaussian Input (.gif) format. DFT calculation using Gaussian 09 WIN 64 using B3LYP/3–21G* basis set and saved the output files as .out. The values of global reactivity parameters were calculated using the energies of HOMO-LUMO in accordance with the Koopmans theorem as given below [45,46]:

Ionization energy (IE) = $-E_{HOMO}$
Electron affinity (EA) = $-E_{LUMO}$
Energy gap (ΔE_g) = $E_{LUMO} - E_{HOMO}$
Electronegativity (χ) = $-(IE + EA)/2$
Chemical potential (μ) = $-\chi$
Chemical hardness (η) = $(IE - EA)/2$
Chemical softness (S) = $1/2\eta$
Global electrophilicity index (ω) = $\mu/2\eta$

CRediT authorship contribution statement

Chander: Writing – original draft, Methodology, Formal analysis, Data curation, Conceptualization. **Monika:** Writing – review & editing, Visualization, Software, Methodology, Data curation, Conceptualization. **Prabhjot Kaur:** Writing – review & editing, Methodology, Formal analysis, Data curation. **Laxmi:** Writing – review & editing. **Neera Raghav:** Validation, Methodology, Investigation, Formal analysis, Data curation. **Pawan K. Sharma:** Writing – review & editing, Investigation. **Sita Ram:** Writing – review & editing, Validation, Supervision, Resources, Methodology, Investigation, Conceptualization.

Declaration of competing interest

The authors declare that they have no known competing financial interests or personal relationships that could have appeared to influence the work reported in this paper.

Data availability

Data will be made available on request.

Acknowledgments

We acknowledge the Department of Science and Technology, India for providing DST PURSE GRANT (Ref no.: SR/PURSE/2022/126) to Dr. Sita Ram and the Council of Scientific and Industrial Research, New Delhi, India, for providing financial assistance to Monika as CSIR-SRF (File no.: 09/ 1256(11466)/2021-EMR-1).

Supplementary materials

Supplementary material associated with this article can be found, in the online version, at doi:10.1016/j.molstruc.2024.139680.

References

[1] S. Chen, H. Dong, H.Guo S.Yang, Cathepsins in digestive cancers, Oncotarget 8 (2017) 41690, https://doi.org/10.18632/oncotarget.16677.
[2] T. Yadati, T. Houben, A. Bitorina, R. Shiri-Sverdlov, The ins and outs of cathepsins: physiological function and role in disease management, Cells 9 (2020) 1679, https://doi.org/10.3390/cells9071679.
[3] T.S. Zamolodchikova, S.M. Tolpygo, E.V. Svirshchevskaya, Cathepsin G - not only inflammation: the immune protease can regulate normal physiological processes, Front. Immunol. 11 (2020) 512219, https://doi.org/10.3389/fimmu.2020.00411.
[4] M. Scarcella, D. d'Angelo, M. Ciampa, S. Tafuri, L. Avallone, L.M. Pavone, V. D. Pasquale, The key role of lysosomal protease cathepsins in viral infections, Int. J. Mol. Sci. 23 (2022) 9089, https://doi.org/10.3390/ijms23169089.
[5] J. Wang, Z. Minying, Y. Xiaohui, Z. Xinyue, Z. Shiwu, The role of Cathepsin B in pathophysiologies of non-tumor and tumor tissues: a systematic review, J. Cancer 14 (2023) 2344, https://doi.org/10.7150/jca.86531.
[6] V. Stoka, V. Turk, B. Turk, Lysosomal cathepsins and their regulation in aging and neurodegeneration, Ageing Res. Rev. 32 (2016) 22–37, https://doi.org/10.1016/j.arr.2016.04.010.
[7] B. Saroha, G. Kumar, P. Arya, N. Raghav, S. Kumar, Some morpholine tethered novel aurones: design, synthesis, biological, kinetic and molecular docking studies, Bioorg. Chem. 140 (2023) 106805.
[8] H. Nakanishi, Microglial cathepsin B as a key driver of inflammatory brain diseases and brain aging, Neural Regen. Res. 15 (2020) 25, https://doi.org/10.1016/j.bioorg.2023.106805.
[9] V. Hook, M. Yoon, C. Mosier, G. Ito, S. Podvin, B.P. Head, R. Rissman, A.J. O. Donoghue, G. Hook, Cathepsin B in neurodegeneration of Alzheimer's disease, traumatic brain injury, and related brain disorders, Biochim. Biophys. Acta, Proteins Proteomics 1868 (2020) 140428, https://doi.org/10.1016/j.bbapap.2020.140428.
[10] B. Saroha, G. Kumar, M. Kumari, R. Kaur, N. Raghav, P.K. Sharma, N. Kumar, S. Kumar, A decennary update on diverse heterocycles and their intermediates as privileged scaffolds for cathepsin B inhibition, Int. J. Biol. Macromol. 222 (2022) 2270–2308, https://doi.org/10.1016/j.ijbiomac.2022.10.017.
[11] D. Dixit, P.K. Verma, R.K. Marwaha, A review on 'triazoles': their chemistry, synthesis and pharmacological potentials, J. Iran. Chem. Soc. 18 (2021) 2535–2565, https://doi.org/10.1007/s13738-021-02231-x.
[12] M. Luczynski, A. Kudelko, Synthesis and biological activity of 1,3,4-oxadiazoles used in medicine and agriculture, Appl. Sci. 12 (2022) 3756, https://doi.org/10.3390/app120837, 56.
[13] K. Siwach, M. Rani, L. Vats, S. Giovannuzzi, A.K. Paul, M. Brahma, N. Kumari, M. Maruthi, N. Raghav, C.T. Supuran, P.K. Sharma, 1, 2, 3-Triazole-based esters and carboxylic acids as nonclassical carbonic anhydrase inhibitors capable of cathepsin B inhibition, Arch. Pharm 357 (2023) e2300372, https://doi.org/10.1002/ardp.202300372.
[14] B. Saroha, G. Kumar, S. Kumar, M. Kumari, M. Rani, N. Raghav, P.K. Sahoo, S. Ghosh, S. Mahata, V.D. Nasare, Novel 1, 2, 3-triazole-aurone hybrids as cathepsin B inhibitors: one-pot synthesis, anti-proliferative, and drug modeling studies, Eur. J. Med. Chem. Reports 5 (2022) 100056, https://doi.org/10.1016/j.ejmcr.2022.100056.
[15] B. Saroha, G. Kumar, S. Kumar, M. Kumari, M. Rani, N. Raghav, P.K. Sahoo, S. Ghosh, S. Mahata, V.D. Nasare, Ultrasound assisted a one pot multicomponent and greener synthesis of 1, 2, 3-triazole incorporated aurone hybrids: cathepsin B inhibition, anti-cancer activity against AGS cell line, and in-silico docking evaluation, Curr. Res. Green Sustain. Chem. 5 (2022) 100295, https://doi.org/10.1016/j.crgsc.2022.100295.
[16] S. Garg, N. Raghav, 2, 5-Diaryloxadiazoles and their precursors as novel inhibitors of cathepsins B, H and L, Bioorg. Chem. 67 (2016) 64–74, https://doi.org/10.1016/j.bioorg.2016.05.003.
[17] M. Abdoli, V. Krasniqi, A. Bonardi, M. Gütschow, C.T. Supuran, R. Žalubovskis, 4-Cyanamido-substituted benzenesulfonamides act as dual carbonic anhydrase and cathepsin inhibitors, Bioorg. Chem. 139 (2023) 106725, https://doi.org/10.1016/j.bioorg.2023.106725.
[18] L. Vats, P. Arya, R. Kumar, S. Giovannuzzi, N. Raghav, C.T. Supuran, P.K. Sharma, Keto-bridged dual triazole-linked benzenesulfonamides as potent carbonic anhydrase and cathepsin B inhibitors, Future Med. Chem. 15 (2023) 1843–1863, https://doi.org/10.4155/fmc-2023-0201.
[19] A. Kumar, P. Arya, V. Sharma, S. Giovannuzzi, N. Raghav, C.T. Supuran, P. K. Sharma, Potent inhibitors of tumor associated carbonic anhydrases endowed with cathepsin B inhibition, Arch. Pharm. 356 (2023) 2300349, https://doi.org/10.1002/ardp.202300349.
[20] B.J. Bender, S. Gahbauer, A. Luttens, J. Lyu, C.M. Webb, R.M. Stein, E.A. Fink, T. E. Balius, J. Carlsson, J.J. Irwin, B.K. Soichet, A practical guide to large-scale docking, Nat. Protoco. 16 (2021) 4799–4832, https://doi.org/10.1038/s41596-021-00597-z.
[21] D. Sahin, R.A. Kepekci, M.F. Dehnayebi, S. Akkoc, J.V.C. Vicario, N. Micale, Biological activities, DFT calculations, and molecular docking simulation of thymol-based compounds, Chemistryselect 9 (2024) e202304572, https://doi.org/10.1002/slct. 202304572.
[22] G. Kumar, P. Kumar, A. Soni, V. Sharma, M. Nemiwal, Efficient synthesis and molecular docking analysis of quinazoline and azole hybrid derivatives as promising agents for anti-cancer and anti-tuberculosis activities, J. Mol. Struct. 1310 (2024) 138289, https://doi.org/10.1016/j.molstruc.2024.138289.
[23] M. Sundari, A. Jha, K.R. Amperayani, V.M. Chand, Design, ultrasonic synthesis, antimicrobial activity and molecular docking studies of pyridine-2,6-dithiazole/dioxazole analogues, J. Mol. Struct. 1316 (2024) 139063.
[24] F. Stanzione, I. Giangraco, J.C. Cole, Chapter Four - Use of molecular docking computational tools in drug discovery, Prog. Med. Chem. 60 (2021) 272–343, https://doi.org/10.1016/bs.pmch.2021.01.004.
[25] J. Fan, A. Fu, L. Zhang, Progress in molecular docking, Quant. Biol. 7 (2019) 83–89, https://doi.org/10.1007/s40484-019-0172-y.
[26] B.G.D. Rio, B. Phan, R. Ramprasad, A deep learning framework to emulate density functional theory, Npj Comput. Mater. 9 (2023) 158, https://doi.org/10.1038/s41524-023-01115-3.
[27] Y. Ding, Y. Zhang, L. Yan, L. Liu, New pyrimidinothiophene derivatives: synthesis, spectroscopic analysis, X-ray, DFT calculation, biological activity studies and ADMET prediction, J. Mol. Struct. 1290 (2023) 135952, https://doi.org/10.1016/j.molstruc.2023.135952.
[28] T. Liu, J. Chen, C. Fan, C. Wu, T. Sun, Crystal structure, DFT calculation, molecular docking, in vitro biological activity evaluation and in silico drug-likeness prediction of (E)-N-(4-bromophenyl)-4-(2-(2-hydroxybenzylidene) hydrazine-1-carbonyl) benzenesulfonamide, J. Mol. Struct. 1284 (2023) 135319, https://doi.org/10.1016/j.molstruc.2023.135319.
[29] K.E. Anwer, Z.B. Hamza, R.M. Ramadan, Synthesis, spectroscopic, DFT calculations, biological activity, SAR, and molecular docking studies of novel bioactive pyridine derivatives, Sci. Rep. 13 (2023) 15598, https://doi.org/10.1038/s41598-023-42714-w.
[30] A. Zochedh, M. Priya, A. Shunmuganarayanan, K. Thandavarayan, A.B. Sultan, Investigation on structural, spectroscopic, DFT, biological activity and molecular docking simulation of essential oil Gamma-Terpinene, J. Mol. Struct. 1268 (2022) 133651, https://doi.org/10.1016/j.molstruc.2022.133651.
[31] M.M. Alam, A.S. Almalki, T. Neamatallah, N.M. Ali, A.M. Malebari, S. Nazreen, Synthesis of new 1, 3, 4-oxadiazole-incorporated 1, 2, 3-triazole moieties as potential anticancer agents targeting thymidylate synthase and their docking studies, Pharmaceuticals 13 (2020) 390, https://doi.org/10.3390/ph13110390.
[32] N. Batra, V. Rajendran, I. Wadi, A. Lathwal, R.K. Dutta, P.C. Ghosh, R.D. Gupta, M. Nath, Synthesis, characterization, and antiplasmodial efficacy of sulfonamide-appended [1, 2, 3]-triazoles, J. Het. Chem. 57 (2020) 1625–1636, https://doi.org/10.1002/jhet.3888.
[33] N. Raghav, N. Mor, Study on enhanced serum protein protecting and anti-cathepsin activities of various curcumin formulations containing traditional excipients and bio-enhancers, Bioorg. Chem. 104 (2020) 104177, https://doi.org/10.1016/j.bioorg.2020.104177.
[34] M. Mohanty, P.S. Mohanty, Molecular docking in organic, inorganic, and hybrid systems: a tutorial review, Monatsh. Chem. 154 (2023) 683–707, https://doi.org/10.1007/s00706-023-03076-1.
[35] I. Caracelli, M. Vega-Teijido, J. Zukerman-Schpector, M.H. Cezari, J.G. Lopes, L. Juliano, P.S. Santosh, J.V. Comasetto, R.L. Cunha, E.R. Tiekink, A tellurium-based cathepsin B inhibitor: molecular structure, modelling, molecular docking and biological evaluation, J. Mol.Struct. 1013 (2012) 11–18, https://doi.org/10.1016/j.molstruc.2012.01.008.
[36] K.E. Gadali, M. Rafya, A.E. Mansouri, M. Maatallah, A. Vanderlee, A. Mehdi, J. Neyts, D. Jochmans, S.D. Jonhge, F. Benkhalti, Y.S. Sanghvi, M. Taourirte, H. B. Lazrek, Design, synthesis, and molecular modeling studies of novel 2-quinolone-1,2,3-triazole-α-aminophosphonates hybrids as dual antiviral and antibacterial agents, Eur. J. Med. Chem. 268 (2024) 116235, https://doi.org/10.1016/j.ejmech.2024.116235.
[37] I. Ravish, N. Raghav, Curcumin as inhibitor of mammalian cathepsin B, cathepsin H, acid phosphatase and alkaline phosphatase: a correlation with pharmacological activities, Med. Chem. Res. 23 (2014) 2847–2855, https://doi.org/10.1007/s00044-013-0872-1.
[38] N. Raghav, R. Kaur, Synthesis and evaluation of some semicarbazone-and thiosemicarbazone-based cathepsin B inhibitors, Med. Chem. Res. 23 (2014) 4669–4679, https://doi.org/10.1007/s00044-014-1036-7.
[39] C. Vashisth, T. Kaushik, N. Vashisth, N. Raghav, Cinnamaldehyde hydrazone derivatives as potential cathepsin B inhibitors: a parallel in-vitro investigation in liver and cerebrospinal fluid, Int. J. Biol. Macromol. 272 (2024) 132684, https://doi.org/10.1016/j.ijbiomac.2024.132684.
[40] N. Chitranshi, V.K. Gupta, R. Rajput, A. Godinez, K. Pushpitha, T. Shen, M. Mirzaei, Y. You, D. Basavarajappa, V. Gupta, S.L. Graham, Evolving geographic diversity in SARS-CoV2 and in silico analysis of replicating enzyme 3CL(pro) targeting repurposed drug candidates, J. Transl. Med. 18 (2020) 278, https://doi.org/10.1186/s12967-020-02448-z.

[41] G.M. Morris, D.S. Goodsell, R.S. Halliday, R. Huey, W.E. Hart, R.K. Belew, A. J. Olson, Automated docking using a Lamarckian genetic algorithm and an empirical binding free energy function, J. Comput. Chem. 19 (1998) 1639–1662.
[42] N. Chitranshi, A. Kumar, S. Sheriff, V. Gupta, A. Godinez, D. Saks, S. Sarkar, T. Shen, M. Mirzaei, D. Basavarajappa, M. Abyadeh, S.K. Singh, K. Dua, K.Y. J. Jhang, S.L. Graham, V. Gupta, Identification of novel cathepsin B inhibitors with implications in Alzheimer's disease: computational refining and biochemical evaluation, Cells 10 (2021) 1946.
[43] P.D. Greenspan, K.L. Clark, R.A. Tommasi, S.D. Cowen, L.W. McQuire, D.L. Farley, J.H. VanDuzer, R.L. Goldberg, H. Zhou, Z. Du, J.J. Fitt, D.E. Coppa, Z. Fang, W. Macchia, L. Zhu, M.P. Capparelli, R. Goldstein, A.M. Wigg, J.R. Doughty, R. S. Bohacek, A.K. Knap, Identification of dipeptidyl nitriles as potent and selective inhibitors of cathepsin B through structure-based drug design, J. Med. Chem. 44 (2001) 4524–4534.
[44] S. Armakovic, S.J. Armakovic, Atomistica.online – web application for generating input files for ORCA molecular modelling package made with the Anvil platform, Mol. Simul. 49 (2023) 117–123.
[45] C.I. Oprea, M.A. Girtu, Structure and electronic properties of TiO_2 nanoclusters and dye–nanocluster systems appropriate to model hybrid photovoltaic or photocatalytic applications, Nanomaterials 9 (2019) 357.
[46] A.B. Cassalas, C. Quiroga, C. Ortiz, D. Benitez, P.A. Denis, D. Figueroa, C.O. Salas, J. Bertrand, R.A. Topia, P. Sanchez, G.P. Miscione, M.A. Comini, M. Paulino, Mode of action of *p*-quinone derivatives with trypanocidal activity studied by experimental and *in silico* models, Eur. J. Med. Chem. 246 (2023) 114926.